Effects of the local resonance on the wave propagation in periodic frame structures: Generalized Newtonian mechanics

Céline Chesnais[a)]
Université Paris-Est, IFSTTAR, GER, F-75732, Paris, France

Claude Boutin and Stéphane Hans
DGCB, FRE CNRS 3237, École Nationale des Travaux Publics de l'État, Université de Lyon, France

(Received 15 February 2012; revised 4 July 2012; accepted 16 July 2012)

This work is devoted to the study of the wave propagation in infinite two-dimensional structures made up of the periodic repetition of frames. Such materials are highly anisotropic and, because of lack of bracing, can present a large contrast between the shear and compression deformabilities. Moreover, when the thickness to length ratio of the frame elements is small, these elements can resonate in bending at low frequencies when compressional waves propagate in the structure. The frame size being small compared to the wavelength of the compressional waves, the homogenization method of periodic discrete media is extended to situations with local resonance, and it is applied to identify the macroscopic behavior at the leading order. In particular, the local resonance in bending leads to an effective mass different from the real mass and to the generalization of the Newtonian mechanics at the macroscopic scale. Consequently, compressional waves become dispersive and frequency bandgaps occur. The physical origin of these phenomena at the microscopic scale is also presented. Finally, a method is proposed for the design of such materials.
 [http://dx.doi.org/10.1121/1.4744975]

PACS number(s): 43.20.Bi, 43.20.Ks, 43.40.At [ANN] Pages: 2873–2886

I. INTRODUCTION

Two considerations may explain the great number of studies devoted to the dynamic properties of periodic reticulated (or cellular) structures, namely structures obtained by repeating a unit cell made up of interconnected beams (or plates). The first reason is that they are frequently encountered. For example, they appear in sandwich panels, stiffened plates, and truss beams used in aerospace and marine structures. They can also represent idealized buildings or the microstructure of foams, plants, bones,…. The second reason is that the dynamic behavior of periodic materials is very rich. They are known for the existence of frequency bandgaps, that is to say, intervals of frequencies at which wave propagation cannot occur.[1,2] Moreover, in pass bands, waves travel in preferred directions[3–5] because of the anisotropy. In most cases, frequency bandgaps are caused by Bragg scattering when the wavelength is on the order of the cell size. This corresponds to the framework of phononic crystals. However, frequency bandgaps can also appear at wavelengths much greater than the cell size, which defines the notion of metamaterials. This was evidenced theoretically in the pioneering Ref. 6 by considering an elastic composite with a high contrast between the rigidities of the two constituents and in Ref. 7 for lattices. The consequence of the rigidity contrast is that the softer component resonates at low frequencies when macroscopic waves propagate in the stiffer component. The effects of the local resonance were also observed experimentally.[8,9] Metamaterials have unusual properties.[10] In particular, at the macroscopic scale, the effective mass differs from the real mass. It depends on the frequency, which leads to non-local effects in time. Therefore the description of the behavior at the macroscopic scale is a generalization of the Newtonian mechanics.[11] Metamaterials represent a specific class of generalized continua. A review of recent advances on this topic can be found in Ref. 12.

This work analyzes the propagation of plane waves in two-dimensional periodic structures the unit cell of which is a frame (Fig. 1). Such materials are highly anisotropic because the resisting elements are oriented only according two directions. Also the elements are more flexible in bending than in tension-compression. As the frames are not braced, the shear deformability is much greater than the compression deformability. Moreover, when the thickness to length ratio of the elements is small, they can resonate in bending at low frequencies. In that case, the propagation of compressional waves with a wavelength much greater than the cell size can induce the resonance of the elements in bending. This phenomenon makes it possible to realize metamaterials with only one constituent contrary to the other metamaterials based on the stiffness contrast between the different components. The objective is the description of the behavior of the structure at the macroscopic scale and the research of its physical origin at the microscopic scale. This enables to identify the conditions of existence of atypical behaviors and to propose a method for the design of new materials.

Specific numerical methods have been developed for the study of the wave propagation in periodic media.[1,2,5] They are based on the Floquet–Bloch theorem, which enables to reduce the study of the whole structure to the study of the unit cell. Another approach consists in replacing a discrete structure by an equivalent continuum.[13–15] When the wavelength is much greater than the cell size, it is possible to use

a)Author to whom correspondence should be addressed. Electronic mail: celine.chesnais@ifsttar.fr

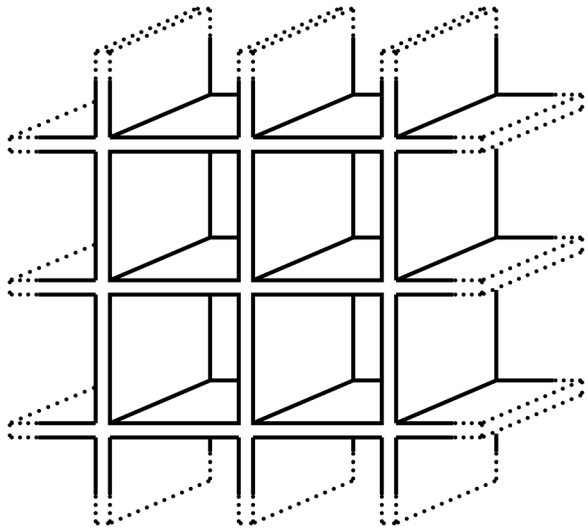

FIG. 1. Example of structures.

the rigorous asymptotic methods of homogenization that require no assumption about the nature of the continuum. Earlier works can be found in Refs. 16 and 17 for composite media and in Ref. 18 for reticulated structures. The method was also successfully applied to the study of Rayleigh scattering in periodic media.[19] For reticulated structures, the physics of the unit cell can be described either using the continuum mechanics as in the method of multiple parameters and scale changes[20,21] or using the beam theory as in the homogenization method of periodic discrete media.[22,23] Other procedures that extend homogenization to higher frequencies can be found in Refs. 24 and 25 for continuous structures and in Ref. 26 for discrete mass-spring systems.

Here, the homogenization method of periodic discrete media (HPDM) is used. This method has already given interesting results on the dynamic behavior of frame structures in the absence of local resonance.[27,28] Its main advantages are:

(1) The equivalent continuum (a Cauchy continuum, a generalized medium or a metamaterial) is derived rigorously from the properties of the cell. The only assumption is scale separation, which means that two scales with very different characteristic lengths can be defined. The macroscopic or global scale is given by the wave propagation and the microscopic or local scale is given by the size of the cell.
(2) The method is completely analytic. This provides a clear understanding of the mechanisms governing the behavior of the structure and of the role of each parameter. Such a knowledge is desirable for the design of new (meta)materials with prescribed properties.
(3) Once the macroscopic behavior is identified, it is always possible to come back to the microscopic scale to determine the deformation of the cell as well as the forces and moments in the elements.
(4) Superior orders of the expansions are obtained relatively easily. This is particularly interesting for frame structures because the shear stiffness and the tension-compression stiffness do not have the same order of magnitude. Because the method of multiple parameters and scale changes is generally limited to the leading order, it misses the shear properties and the coerciveness of the macroscopic description is lost.[21]

The implementation of the HPDM method is realized in two steps[23]: the discretization of the momentum balance and the homogenization process itself. As in Refs. 27 and 28, the HPDM method is coupled with the scaling of all the parameters to correctly take into account the physics of the problem. Moreover, the homogenization process has been adapted to situations with local resonance.[42]

Section II describes the studied structures and the principles of the HPDM method. Then the equivalent continuum obtained in the absence of local resonance is presented in Sec. III. In Secs. IV and V, the wave propagation is analyzed at two frequency ranges. The first case corresponds to the classical domain of homogenization, whereas the second case deals with local resonance. The application of the results to real frame structures is discussed in Sec. VI, and a method is proposed for the design of metamaterials.

II. HOMOGENIZATION OF PERIODIC DISCRETE MEDIA

A. Studied structures

The studied structures are infinite and periodic in the plane (x, y) of the wave propagation. They are made up of horizontal elements (called floors) supported by vertical elements (called walls). Elements are beams or plates behaving as Euler–Bernoulli beams in the plane (x, y). They are linked by perfectly stiff and massless nodes. Moreover, the walls and the floors have similar properties. The following notation will be used (Fig. 2):

(1) The characteristics of walls ($i = w$) and floors ($i = f$) are: ℓ_i, length; a_i, thickness; h, depth according to the axis z; $A_i = a_i h$, cross-section area; $I_i = (h a_i^3)/12$, second moment of area with respect to the axis z; ρ_i, density; $\bar{\rho}_i = \rho_i A_i$, mass per unit length; and E_i, elastic modulus.
(2) The position of the node located at the intersection of the floor f and the wall w is determined either by the ordered pair of integers (w, f) or by the continuous coordinates $x = w\ell_f$ and $y = f\ell_w$.

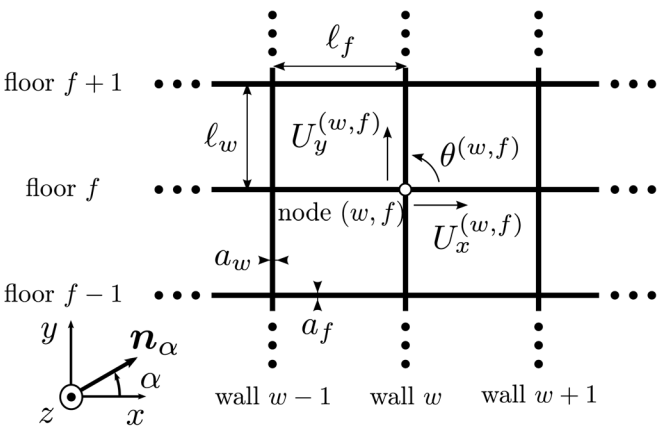

FIG. 2. Notation (structure).

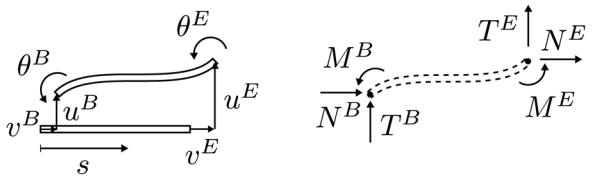

FIG. 3. Notation (element).

(3) As the connections are perfectly stiff, the motions of each endpoint connected to the same node are identical and define the discrete kinematic variables of the system. For the node (w, f), the motion in the plane (x, y) is described by the displacements in the two directions $U_x^{(w,f)}$, $U_y^{(w,f)}$ and by the rotation $\theta^{(w,f)}$.

The study is conducted within the framework of the small strain theory and the linear elasticity. Moreover, the structure vibrates at a given circular frequency ω. As a result, every variable can be written in the following way: $X(x, y, t) = \Re(X(x, y)e^{i\omega t})$ where t is the time. Because of the linearity of the problem, the time dependence can be simplified and will be systematically omitted.

B. Discretization of the dynamic balance

The aim of the first step is to reduce the study of the momentum balance of the whole structure to the study of the momentum balance of the nodes. This process is performed without loss of information. The discretization consists in expressing explicitly the forces at the endpoints of an element as functions of the nodal kinematic variables. Then the balance of forces and moments applied by the elements connected to a same node is written, and these equations constitute the discrete description of the dynamic behavior of the structure. The process is detailed afterward.

The element linking the node B to the node E is considered (Fig. 3). It is characterized by the parameters ℓ, A, and I. In the local beam frame, s stands for the coordinate along the beam axis, u, v for the transverse and axial displacements, respectively, and θ for the rotation. The primes denote the differentiation with respect to s. The axial force N, the shear force T, and the bending moment M act by convention from the left part to the right part. No external force is applied on the beam.

The longitudinal vibrations in harmonic regime are described by the momentum balance along the beam axis and by the compression constitutive law:

$$\begin{cases} N'(s) = \rho A\omega^2 v(s) \\ N(s) = -EA\, v'(s) \end{cases} \Rightarrow \begin{array}{l} v''(s) = -\chi^2 v(s) \\ \text{where } \chi = \sqrt{\dfrac{\rho\omega^2}{E}} = \dfrac{2\pi}{\lambda_c}. \end{array}$$

λ_c is the compression wavelength in the element at the studied circular frequency ω.

The transverse vibrations are described by the momentum balance along the transverse axis, the moment of momentum balance, and the bending constitutive law:

$$\begin{cases} T'(s) = \rho A\omega^2 u(s) \\ M'(s) = -T(s) \\ M(s) = -EI\, u''(s) \end{cases} \Rightarrow \begin{array}{l} u''''(s) = \beta^4 u(s) \\ \text{where } \beta = \sqrt[4]{\dfrac{\rho A\omega^2}{EI}} = \dfrac{2\pi}{\lambda_b}. \end{array}$$

λ_b is the bending wavelength in the element.

Both wavelengths are related by a purely geometric relationship:

$$\lambda_b^2 = \lambda_c 2\pi\sqrt{\frac{I}{A}} = \lambda_c \frac{2\pi a}{\sqrt{12}} \Rightarrow \frac{\lambda_b}{\lambda_c} = O\left(\frac{a}{\lambda_b}\right) \ll 1. \quad (1)$$

Indeed, the Euler–Bernoulli beam description requires that the bending wavelength is much greater than the thickness of the element. Thus the bending wavelength is always smaller than the compression wavelength.

The previous equations are now integrated between the nodes B and E using the unknown displacements and rotations of the endpoints (u^B, v^B, θ^B and u^E, v^E, θ^E) as boundary conditions. This provides the expressions of the forces at the extremities of the element in its local frame:

$$\begin{array}{ll} N^B = N(v^B, v^E) & N^E = -N(v^B, v^E) \\ T^B = T(u^B, u^E, \theta^B, \theta^E) & T^E = T(-u^E, -u^B, \theta^E, \theta^B) \\ M^B = M(u^B, u^E, \theta^B, \theta^E) & M^E = M(u^E, u^B, -\theta^E, -\theta^B), \end{array} \quad (2)$$

where

$$N(v_1, v_2) = \frac{EA\chi}{\sin(\chi\ell)}\Big(v_1\cos(\chi\ell) - v_2\Big)$$

$$T(u_1, u_2, \theta_1, \theta_2) = \frac{EI\beta^3}{1-\cos(\beta\ell)\cosh(\beta\ell)}\Big(u_1\Big(\cosh(\beta\ell)\sin(\beta\ell) + \sinh(\beta\ell)\cos(\beta\ell)\Big) - u_2\Big(\sin(\beta\ell) + \sinh(\beta\ell)\Big) + \frac{\theta_1}{\beta}\sin(\beta\ell)\sinh(\beta\ell) - \frac{\theta_2}{\beta}\Big(\cos(\beta\ell) - \cosh(\beta\ell)\Big)\Big)$$

$$M(u_1, u_2, \theta_1, \theta_2) = \frac{EI\beta^2}{1-\cos(\beta\ell)\cosh(\beta\ell)}\Big(u_1\sin(\beta\ell)\sinh(\beta\ell) + u_2\Big(\cos(\beta\ell) - \cosh(\beta\ell)\Big) + \frac{\theta_1}{\beta}\Big(\cosh(\beta\ell)\sin(\beta\ell) - \sinh(\beta\ell)\cos(\beta\ell)\Big) - \frac{\theta_2}{\beta}\Big(\sin(\beta\ell) - \sinh(\beta\ell)\Big)\Big). \quad (3)$$

The dynamic balance of each element being satisfied, it remains to write the balance of the nodes. Because their mass is negligible and there is no external force, it consists in adding the forces (or moments) applied by the four elements (two walls and two floors) connected to the same node. Here the geometry of the structure is explicitly taken into account. In the global frame (x, y) (Fig. 2), the balance of the nodes is:

(1) Balance of momentum in the x direction:

$$\begin{aligned} &T_w^E\left(U_x^{(w,f-1)}, U_x^{(w,f)}, -\theta^{(w,f-1)}, -\theta^{(w,f)}\right) \\ &- T_w^B\left(U_x^{(w,f)}, U_x^{(w,f+1)}, -\theta^{(w,f)}, -\theta^{(w,f+1)}\right) \\ &+ N_f^E\left(U_x^{(w-1,f)}, U_x^{(w,f)}\right) - N_f^B\left(U_x^{(w,f)}, U_x^{(w+1,f)}\right) = 0. \end{aligned} \tag{4a}$$

(2) Balance of momentum in the y direction:

$$\begin{aligned} &N_w^E\left(U_y^{(w,f-1)}, U_y^{(w,f)}\right) - N_w^B\left(U_y^{(w,f)}, U_y^{(w,f+1)}\right) \\ &+ T_f^E\left(U_y^{(w-1,f)}, U_y^{(w,f)}, \theta^{(w-1,f)}, \theta^{(w,f)}\right) \\ &- T_f^B\left(U_y^{(w,f)}, U_y^{(w+1,f)}, \theta^{(w,f)}, \theta^{(w+1,f)}\right) = 0. \end{aligned} \tag{4b}$$

(3) Balance of moment of momentum:

$$\begin{aligned} &M_w^E\left(-U_x^{(w,f-1)}, -U_x^{(w,f)}, \theta^{(w,f-1)}, \theta^{(w,f)}\right) \\ &- M_w^B\left(-U_x^{(w,f)}, -U_x^{(w,f+1)}, \theta^{(w,f)}, \theta^{(w,f+1)}\right) \\ &+ M_f^E\left(U_y^{(w-1,f)}, U_y^{(w,f)}, \theta^{(w-1,f)}, \theta^{(w,f)}\right) \\ &- M_f^B\left(U_y^{(w,f)}, U_y^{(w+1,f)}, \theta^{(w,f)}, \theta^{(w+1,f)}\right) = 0. \end{aligned} \tag{4c}$$

Once the nodal variables have been determined, it is always possible to calculate the forces and displacements inside each element. Therefore the discrete description offered by these finite difference equations is fully equivalent to the complete description.

C. Scale separation and local resonance

The principles of homogenization are now used to derive the differential equations describing the behavior of the equivalent continuum. The key assumption is scale separation. This means that the characteristic length L of the deformation of the structure under vibrations is much greater than the characteristic length ℓ_c of the basic frame. Thus the scale ratio $\epsilon = \ell_c/L$ is a small parameter ($\epsilon \ll 1$), and it is possible to expand the kinematic variables and some forces. In this study, the dimensions of the frame in the x and y directions have the same order of magnitude and $\ell_c = \ell_w$ by convention. The size L is related to the macroscopic wavelength and is unknown for the moment.

If the frequency of the vibrations of the structure is much lower than the natural frequencies of the frame elements, then the condition of scale separation is respected. However, having a quasi-static state at the local scale is only a sufficient condition, and homogenization can sometimes be applied with local resonance. This notion is illustrated by considering a structure vibrating at different ranges of frequency. At very low frequencies, both bending and compression waves generated in the elements have wavelengths much longer than the length of the elements. Consequently, the parameters $\chi\ell$ and $\beta\ell$ are very small:

$$\chi\ell = 2\pi\frac{\ell}{\lambda_c} \ll 1 \text{ and } \beta\ell = 2\pi\frac{\ell}{\lambda_b} \ll 1,$$

and the trigonometrical functions can be expanded in the expressions of the nodal forces and moment [Eq. (3)]:

$$\begin{aligned} N(v_1, v_2) &= \frac{EA}{\ell}\left((v_1 - v_2) - \frac{(\chi\ell)^2}{6}(2v_1 + v_2) - \frac{(\chi\ell)^4}{360}(8v_1 + 7v_2)\right) + O\left((\chi\ell)^6\right) \\ T(u_1, u_2, \theta_1, \theta_2) &= -\frac{12EI}{\ell^3}\left((u_1 - u_2) + \frac{\ell}{2}(\theta_1 + \theta_2) - \frac{(\beta\ell)^4}{840}(26u_1 + 9u_2) - \frac{(\beta\ell)^4\ell}{5040}(22\theta_1 - 13\theta_2)\right) \\ &\quad + O\left((\beta\ell)^8\right) \\ M(u_1, u_2, \theta_1, \theta_2) &= \frac{6EI}{\ell^2}\left((u_1 - u_2) + \frac{\ell}{3}(2\theta_1 + \theta_2) - \frac{(\beta\ell)^4}{2520}(22u_1 + 13u_2) - \frac{(\beta\ell)^4\ell}{2520}(4\theta_1 - 3\theta_2)\right) + O\left((\beta\ell)^8\right). \end{aligned} \tag{5}$$

When the frequency is increased, both wavelengths decrease, but λ_c is always longer than λ_b [see Eq. (1)]. The previous expansions remain valid until the bending wavelength λ_b becomes of the same order as the length of the elements:

$$\ell \approx \frac{\lambda_b}{2\pi} \ll \frac{\lambda_c}{2\pi} \Rightarrow \beta\ell = O(1) \quad \text{and} \quad \chi\ell \ll 1.$$

In that case, elements are in resonance in bending and the expressions (3) have to be kept for the shear force and the bending moment. Nevertheless as the compression wavelength λ_c is much greater, it is still possible to expand the axial force and to apply homogenization. If the frequency is increased again, the method remains valid provided that the two following conditions are respected. First, the compression

wavelength λ_c in the stiffer elements should be much greater than their length ℓ to define a macroscopic scale. Second, the bending wavelength λ_b in the more flexible elements should be much greater than their thickness a to use the Euler–Bernoulli beam model.

Another consequence of scale separation is that nodal motions vary slowly from one node to the next. Therefore the nodal variables can be considered as the discrete values of continuous functions of space variables x and y:

$$U_x^{(w,f)} = U_x(\epsilon, x = w\ell_f, y = f\ell_w)$$
$$U_y^{(w,f)} = U_y(\epsilon, x = w\ell_f, y = f\ell_w)$$
$$\theta^{(w,f)} = \theta(\epsilon, x = w\ell_f, y = f\ell_w).$$

These new functions are assumed to converge as ϵ approaches 0 and are replaced by asymptotic expansions in powers of ϵ:

$$X(\epsilon, x, y) = X^0(x, y) + \epsilon X^1(x, y) + \epsilon^2 X^2(x, y) + \ldots \tag{6}$$

where X stands for U_x, U_y, or θ and X^j are continuous functions of order j. In the sequel, the physically observable variables of a given order in ϵ are written with a tilde: $\tilde{X}^j(x, y) = \epsilon^j X^j(x, y)$.

Equations (4a)–(4c) describing the balance of a node also depend on the motions of the four neighboring nodes. Because the structure is periodic, the distances between the nodes are constant. They are equal to $\ell_w = \epsilon L$ in the vertical direction and to $\ell_f = \epsilon \ell^* L$ where $\ell^* = \ell_f/\ell_w = O(1)$ in the horizontal direction. These values are small with respect to x and y, which enables expressing the variations of the motions with Taylor's series:

$$X^{(w,f\pm1)} = X^0(w\ell_f, f\ell_w) + \epsilon\left(X^1(w\ell_f, f\ell_w) \pm L\frac{\partial X^0}{\partial y}(w\ell_f, f\ell_w)\right) + \ldots$$
$$X^{(w\pm1,f)} = X^0(w\ell_f, f\ell_w) + \epsilon\left(X^1(w\ell_f, f\ell_w) \pm \ell^* L\frac{\partial X^0}{\partial x}(w\ell_f, f\ell_w)\right) + \ldots. \tag{7}$$

This introduces the macroscopic derivatives.

D. Normalization

Normalization consists of scaling the physical parameters (the properties of the elements and the circular frequency) according to the powers of ϵ. It ensures that each mechanical effect appears at the same order whatever the value of ϵ. Thus the same physics is kept at the limit $\epsilon \to 0$, which represents the homogenized model.

The choice of the properties of the elements determines the stiffness contrast and then the possible mechanisms in the structure. Here the frames have similar walls and floors with a thickness to length ratio of order ϵ:

$$\frac{E_f}{E_w} = O(1) \quad \frac{\rho_f}{\rho_w} = O(1) \quad \frac{\ell_f}{\ell_w} = O(1) \quad \frac{h_f}{h_w} = O(1)$$
$$\frac{a_w}{\ell_w} = O(\epsilon) \quad \frac{a_f}{\ell_w} = O(\epsilon). \tag{8}$$

As for the circular frequency, the scaling is imposed by the balance of the elastic and inertia forces at the macroscopic level. If the frequency is underestimated, the structure has a quasi-static behavior. On the contrary, if the frequency is overestimated, displacements vanish because the inertia forces cannot be greater than the elastic forces. Nevertheless, the elastic forces can have two origins: the bending or the tension-compression of the elements, and there are two possibilities for the order of magnitude of the frequency. The reference circular frequency is by convention:

$$\omega_r = \frac{1}{L}\sqrt{\frac{E_w}{\rho_w}}.$$

The two frequency ranges of interest are $\omega = O(\epsilon\omega_r)$ and $\omega = O(\omega_r)$.

E. Macroscopic description

Finally, the expansions in powers of ϵ [Eqs. (5)–(7)] and the scaling of the parameters [Eq. (8)] are introduced in Eq. (4) describing the balance of the nodes. The relations obtained being valid for any small enough ϵ, the orders can be separated. This leads to a set of differential equations for each order, which can be solved in increasing order.

The homogenized model is given by the leading order, which corresponds to the limit when ϵ approaches zero. However, in a real structure, the macroscopic length L and the microscopic length ℓ_c are finite, and the physical scale ratio $\tilde{\epsilon}$ is necessarily a finite quantity. Consequently, the kinematic variables of order 0 ($\tilde{U}_x^0$, $\tilde{U}_y^0$, and $\tilde{\theta}^0$) are an approximation of the real motion (the accuracy of which depends on the order of magnitude of $\tilde{\epsilon}$). The terms of superior orders are correctors that improve the accuracy of the macroscopic description by taking into account phenomena of lesser importance.

The following sections focus on the leading order. First the equivalent continuum is characterized and then the wave propagation is studied. To simplify the equations, some macroscopic parameters are defined. They are integrated over the depth of the elements h_w and h_f so that they do not have the usual units.

$M_w = \bar{\rho}_w/\ell_f$: contribution of the walls to the mass per unit surface (kg/m^2)
$M_f = \bar{\rho}_f/\ell_w$: contribution of the floors to the mass per unit surface (kg/m^2)
$M_s = M_w + M_f$: mass per unit surface (kg/m^2)
$E_x = E_f A_f/\ell_w$: elastic modulus in the x direction (N/m)
$E_y = E_w A_w/\ell_f$: elastic modulus in the y direction (N/m)
$G_w = 12\frac{E_w I_w}{\ell_w^2 \ell_f}$: contribution of the walls to the shear modulus (N/m)
$G_f = 12\frac{E_f I_f}{\ell_w \ell_f^2}$: contribution of the floors to the shear modulus (N/m)
$\frac{1}{G} = \frac{1}{G_w} + \frac{1}{G_f}$: shear modulus (N/m)

III. EQUIVALENT CONTINUUM

This section and the next present the behavior of the structure at the lowest circular frequencies giving a dynamic description: $\omega = O(\epsilon\omega_r)$. In that case, the implementation of the HPDM method provides the following equations, corresponding to the balance of momentum in the x and y directions for orders 0, 1, 2 and the balance of moment of momentum at the leading order.

$$\begin{cases} E_x \dfrac{\partial^2 \tilde{U}_x^0}{\partial x^2} = 0 & (x0) \\ E_x \dfrac{\partial^2 \tilde{U}_x^1}{\partial x^2} = 0 & (x1) \\ E_x \dfrac{\partial^2 \tilde{U}_x^2}{\partial x^2} + G_w \left(\dfrac{\partial \tilde{\theta}^0}{\partial y} + \dfrac{\partial^2 \tilde{U}_x^0}{\partial y^2} \right) & (x2) \\ \quad + M_s \omega^2 \tilde{U}_x^0 = 0 \end{cases}$$

$$\begin{cases} E_y \dfrac{\partial^2 \tilde{U}_y^0}{\partial y^2} = 0 & (y0) \\ E_y \dfrac{\partial^2 \tilde{U}_y^1}{\partial y^2} = 0 & (y1) \\ E_y \dfrac{\partial^2 \tilde{U}_y^2}{\partial y^2} + G_f \left(-\dfrac{\partial \tilde{\theta}^0}{\partial x} + \dfrac{\partial^2 \tilde{U}_y^0}{\partial x^2} \right) & (y2) \\ \quad + M_s \omega^2 \tilde{U}_y^0 = 0 \end{cases}$$

$$\left\{ G_w \left(\tilde{\theta}^0 + \frac{\partial \tilde{U}_x^0}{\partial y} \right) - G_f \left(-\tilde{\theta}^0 + \frac{\partial \tilde{U}_y^0}{\partial x} \right) = 0 \quad (m0). \right. \tag{9}$$

The equations according to the x and y directions describe the balance of the forces per unit surface, which suggests using the notion of stress as in continuum mechanics. The normal stress in the x direction σ_{xx}, the normal stress in the y direction σ_{yy}, the shear stresses τ_{xy} and τ_{yx} are defined by:

$$\begin{aligned} \sigma_{xx}(\boldsymbol{U}) &= E_x \frac{\partial U_x}{\partial x} = E_x \epsilon_{xx}(\boldsymbol{U}) \\ \sigma_{yy}(\boldsymbol{U}) &= E_y \frac{\partial U_y}{\partial y} = E_y \epsilon_{yy}(\boldsymbol{U}) \\ \tau_{xy}(\theta, \boldsymbol{U}) &= G_w \left(\theta + \frac{\partial U_x}{\partial y} \right) = \epsilon^2 \hat{\tau}_{xy}(\theta, \boldsymbol{U}) \\ \tau_{yx}(\theta, \boldsymbol{U}) &= G_f \left(-\theta + \frac{\partial U_y}{\partial x} \right) = \epsilon^2 \hat{\tau}_{yx}(\theta, \boldsymbol{U}), \end{aligned} \tag{10}$$

where σ_{xx}, σ_{yy}, $\hat{\tau}_{xy}$, and $\hat{\tau}_{yx}$ have the same order of magnitude and $\boldsymbol{U}$ denotes the displacement vector. Taking $\boldsymbol{U} = \boldsymbol{U}^0 + \epsilon \boldsymbol{U}^1 + \epsilon^2 \boldsymbol{U}^2$ and adding, on the one hand, the $(x0)$, $(x1)$, $(x2)$ of Eq. (9), and, on the other hand, the $(y0)$, $(y1)$, $(y2)$ of Eq. (9), yield the Cauchy's equations of motion valid up to the ϵ^2 order:

$$\begin{cases} \dfrac{\partial \sigma_{xx}}{\partial x} + \dfrac{\partial \tau_{xy}}{\partial y} + M_s \omega^2 U_x = o(\epsilon^2) \\ \dfrac{\partial \tau_{yx}}{\partial x} + \dfrac{\partial \sigma_{yy}}{\partial y} + M_s \omega^2 U_y = o(\epsilon^2). \end{cases}$$

Moreover, as in continuum mechanics, the balance of moment of momentum described by the $(m0)$ of Eq. (9) implies that $\tau_{xy}(\tilde{\theta}^0, \tilde{\boldsymbol{U}}^0) = \tau_{yx}(\tilde{\theta}^0, \tilde{\boldsymbol{U}}^0)$. Therefore it is possible to eliminate the node rotation $\tilde{\theta}^0$:

$$\tilde{\theta}^0 = \frac{G_f}{G_w + G_f} \frac{\partial \tilde{U}_y^0}{\partial x} - \frac{G_w}{G_w + G_f} \frac{\partial \tilde{U}_x^0}{\partial y}, \tag{11}$$

which leads to the usual expression of the shear stresses.

$$\tau_{xy}(\tilde{\theta}^0, \tilde{\boldsymbol{U}}^0) = \tau_{yx}(\tilde{\theta}^0, \tilde{\boldsymbol{U}}^0) = G \left(\frac{\partial \tilde{U}_y^0}{\partial x} + \frac{\partial \tilde{U}_x^0}{\partial y} \right).$$

The expression of the shear modulus G (given in Sec. II E) shows that G is built from the combination of G_w and G_f as springs in series.

After the elimination of $\tilde{\theta}^0$, $(x2)$ and $(y2)$ of Eq. (9) become:

$$\begin{aligned} & E_x \frac{\partial^2 \tilde{U}_x^2}{\partial x^2} + G \left(\frac{\partial^2 \tilde{U}_y^0}{\partial y \partial x} + \frac{\partial^2 \tilde{U}_x^0}{\partial y^2} \right) + M_s \omega^2 \tilde{U}_x^0 = 0 \quad (x2) \\ & E_y \frac{\partial^2 \tilde{U}_y^2}{\partial y^2} + G \left(\frac{\partial^2 \tilde{U}_y^0}{\partial x^2} + \frac{\partial^2 \tilde{U}_x^0}{\partial x \partial y} \right) + M_s \omega^2 \tilde{U}_y^0 = 0 \quad (y2). \end{aligned} \tag{12}$$

The main feature of the macroscopic medium is its extreme anisotropy due to the large difference in magnitude of the moduli E_x, E_y, and G. Because of the quasi-static state at the local scale, the moduli only depend on the *elastostatic* properties of the frame elements. The two elastic moduli, E_x and E_y, are related to the tension-compression rigidity of the floors and to the one of the walls, respectively. On the contrary, the shear mechanism results from the bending of the walls and the floors connected in series. Because beams are far less stiff in bending, the shear modulus G is much less than the elastic moduli:

$$\frac{G}{E_x} = O(\epsilon^2) \quad \frac{G}{E_y} = O(\epsilon^2).$$

This is the reason why it is necessary to calculate equations up to order 2.

Although the shear modulus and the elastic moduli have different orders of magnitude, the equivalent continuum appears as a *"classical" continuum* in the sense that only the translational motion appears at the leading order. The macroscopic behavior is completely described by Eqs. $(x0)$, $(x1)$, $(y0)$, $(y1)$ of Eq. (9), and Eq. (12), which do not contain $\tilde{\theta}^0$. The node rotation has the status of a "hidden" variable. However, to come back to the local scale and to determine

the forces and the displacements in the frame elements, it is necessary to calculate $\tilde{\theta}^0$ with Eq. (11) describing the inner equilibrium of the basic frame.

Finally, note that the previous description of the macroscopic medium established for circular frequencies such that $\omega = O(\epsilon\omega_r)$ remains valid as long as the frame elements are not in resonance in bending. In particular, it applies to statics.

IV. SHEAR WAVES

The wave propagation in the medium is now analyzed. Because every wave can be expressed as a superposition of plane waves, the study focuses on this kind of waves and the displacement field is sought in the following way (remember that the time dependence $\exp(i\omega t)$ is systematically omitted):

$$\boldsymbol{U}(\epsilon, \boldsymbol{x}) = \boldsymbol{u}^0 \exp[-ik(\alpha)\boldsymbol{n}_\alpha \cdot \boldsymbol{x}] + \epsilon \boldsymbol{U}^1(\boldsymbol{x}) + \epsilon^2 \boldsymbol{U}^2(\boldsymbol{x}) + \ldots. \tag{13}$$

Only the expression of the displacement field in the homogenized medium $\boldsymbol{U}^0(\boldsymbol{x}) = \boldsymbol{u}^0 \exp[-ik(\alpha)\boldsymbol{n}_\alpha \cdot \boldsymbol{x}]$ is imposed. It corresponds to a plane wave with amplitude $\boldsymbol{u}^0$ and wave number $k(\alpha)$ traveling in direction $\boldsymbol{n}_\alpha$ (Fig. 2). The correctors could be determined without any assumptions by the resolution of the equations of superior orders as in Ref. 19. Their study is out of the scope of this paper, but the following property will be used. As the medium is infinite and the macroscopic field $\boldsymbol{U}^0$ is invariant under a translation perpendicular to the direction of propagation, the correctors should also be invariant under such a translation.

Expression (13) is introduced in $(x0)$ and $(y0)$ of Eq. (9):

$$\begin{aligned} &-E_x k^2(\alpha)\cos^2(\alpha)\tilde{u}_x^0 \exp[-ik(\alpha)\boldsymbol{n}_\alpha \cdot \boldsymbol{x}] = 0 \quad (x0) \\ &-E_y k^2(\alpha)\sin^2(\alpha)\tilde{u}_y^0 \exp[-ik(\alpha)\boldsymbol{n}_\alpha \cdot \boldsymbol{x}] = 0 \quad (y0). \end{aligned} \tag{14}$$

For $\cos(\alpha) \neq 0$ and $\sin(\alpha) \neq 0$, the only solution is $\boldsymbol{u}^0 = 0$. At this frequency range, waves cannot propagate diagonally.

For $\cos(\alpha) = 0$, $(y0)$ of Eq. (14) implies that $\tilde{u}_y^0 = 0$ and the expression of $\boldsymbol{U}^0$ becomes:

$$\boldsymbol{U}^0(x) = \begin{pmatrix} \tilde{u}_x^0 \\ 0 \end{pmatrix} \exp[\pm ik(\pi/2)y]. \tag{15}$$

This means that the direction of propagation is y (direction of the walls) and the direction of polarization is x (direction of the floors): it is a pure shear wave. To determine the wave number $k(\pi/2)$, expression (15) is introduced in $(x2)$ of Eq. (12):

$$E_x \frac{\partial^2 \tilde{U}_x^2}{\partial x^2} + (-Gk^2(\pi/2) + M_s\omega^2)\tilde{u}_x^0 \exp[\pm ik(\pi/2)y] = 0,$$

and the invariance of the corrector under a translation parallel to the x direction is used:

$$\frac{\partial^2 \tilde{U}_x^2}{\partial x^2} = 0 \quad \Rightarrow \quad k(\pi/2) = \omega\sqrt{\frac{M_s}{G}}. \tag{16}$$

For $\sin(\alpha) = 0$, the results are similar but the roles of x and y are reversed. Pure shear waves travel in the x direction and are polarized in the y direction ($\tilde{u}_x^0 = 0$). $(y2)$ of Eq. (12) gives the same expression of the wave number as in the other direction:

$$E_y \frac{\partial^2 \tilde{U}_y^2}{\partial y^2} + (-Gk^2(0) + M_s\omega^2)\tilde{u}_y^0 \exp[\pm ik(0)x] = 0$$

$$\Rightarrow k(0) = \omega\sqrt{\frac{M_s}{G}} = k(\pi/2).$$

To sum up, at low frequencies, waves can only propagate in two directions because of the anisotropy. Nevertheless, the speeds $c(\alpha)$ are identical in both directions:

$$c(\alpha) = \frac{\omega}{k(\alpha)} = \sqrt{\frac{G}{M_s}}.$$

The speed depends on the shear modulus G and the mass M_s as in a classical elastic medium. The expression of G (given in Sec. II E) shows that these waves are generated by the local bending of the elements (Fig. 4).

Note that $\omega = O(\epsilon\omega_r)$ is really the lowest circular frequency giving a dynamic description at the macroscopic scale. For a smaller ω, the inertial term $M_s\omega^2\boldsymbol{U}^0$ is relegated to a higher order and vanishes in balance equations (12).

V. COMPRESSIONAL WAVES AND LOCAL RESONANCE

The circular frequency ω is now increased up to $O(\omega_r)$ to investigate the behavior of the medium when the inertia forces balance the tension-compression forces. For this frequency range, the bending wavelength in the elements λ_b is of the same order as their length ℓ, but the compression wavelength λ_c remains much longer. It corresponds to the situation presented in Sec. II C where homogenization applies with local resonance in bending. This phenomenon is illustrated in Fig. 5, which shows a compressional wave traveling in the x direction. As its wavelength Λ is much greater than the length of the floors ℓ_f, the condition of scale separation is respected. Therefore homogenization can be used even though the propagation of the wave induces the vibration of the walls and their resonance in bending.

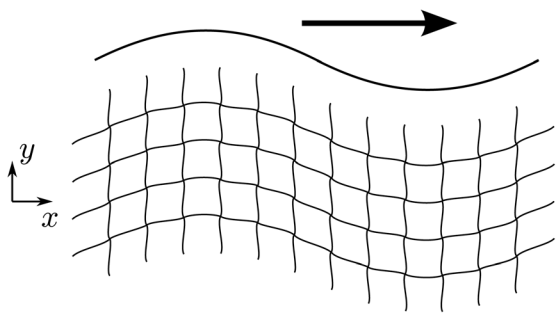

FIG. 4. Shear wave traveling in the x direction.

The consequence of the local resonance is that the shear force and the bending moment in the elements can no longer be expanded contrary to the axial force. The other parts of the HPDM method are unchanged, and the balance of momentum of the macroscopic medium is described by the following equations.

$$E_x \frac{\partial^2 \tilde{U}_x^0}{\partial x^2} + (M_f + M_w f(\hat{\omega}_w))\omega^2 \tilde{U}_x^0 = 0 \qquad (x0)$$

$$E_y \frac{\partial^2 \tilde{U}_y^0}{\partial y^2} + (M_w + M_f f(\hat{\omega}_f))\omega^2 \tilde{U}_y^0 = 0 \qquad (y0)$$

$$\frac{\pi G_w \sqrt{\hat{\omega}_w}}{8 f_e(\hat{\omega}_w)} \left(4 \sin\left(\frac{3\pi}{4}\sqrt{\hat{\omega}_w}\right) \sinh\left(\frac{3\pi}{4}\sqrt{\hat{\omega}_w}\right) \tilde{\theta}^0 + \frac{3\pi\sqrt{\hat{\omega}_w}}{2 f_o(\hat{\omega}_w)} \left(\cosh\left(\frac{3\pi}{2}\sqrt{\hat{\omega}_w}\right) - \cos\left(\frac{3\pi}{2}\sqrt{\hat{\omega}_w}\right) \right) \frac{\partial \tilde{U}_x^0}{\partial y} \right)$$

$$- \frac{\pi G_f \sqrt{\hat{\omega}_f}}{8 f_e(\hat{\omega}_f)} \left(-4 \sin\left(\frac{3\pi}{4}\sqrt{\hat{\omega}_f}\right) \sinh\left(\frac{3\pi}{4}\sqrt{\hat{\omega}_f}\right) \tilde{\theta}^0 + \frac{3\pi\sqrt{\hat{\omega}_f}}{2 f_o(\hat{\omega}_f)} \left(\cosh\left(\frac{3\pi}{2}\sqrt{\hat{\omega}_f}\right) - \cos\left(\frac{3\pi}{2}\sqrt{\hat{\omega}_f}\right) \right) \frac{\partial \tilde{U}_y^0}{\partial x} \right) = 0 \qquad (m0)$$

(17)

with

$$\hat{\omega}_w = \omega \left(\frac{2\ell_w}{3\pi}\right)^2 \sqrt{\frac{\bar{\rho}_w}{E_w I_w}} \approx \frac{\omega}{\omega_{w1}}$$

$$\hat{\omega}_f = \omega \left(\frac{2\ell_f}{3\pi}\right)^2 \sqrt{\frac{\bar{\rho}_f}{E_f I_f}} \approx \frac{\omega}{\omega_{f1}}$$

$$f(\hat{\omega}) = \frac{8}{3\pi\sqrt{\hat{\omega}} f_o(\hat{\omega})} \sin\left(\frac{3\pi}{4}\sqrt{\hat{\omega}}\right) \sinh\left(\frac{3\pi}{4}\sqrt{\hat{\omega}}\right)$$

$$f_o(\hat{\omega}) = \sin\left(\frac{3\pi}{4}\sqrt{\hat{\omega}}\right) \cosh\left(\frac{3\pi}{4}\sqrt{\hat{\omega}}\right) + \sinh\left(\frac{3\pi}{4}\sqrt{\hat{\omega}}\right) \cos\left(\frac{3\pi}{4}\sqrt{\hat{\omega}}\right)$$

$$f_e(\hat{\omega}) = \sin\left(\frac{3\pi}{4}\sqrt{\hat{\omega}}\right) \cosh\left(\frac{3\pi}{4}\sqrt{\hat{\omega}}\right) - \sinh\left(\frac{3\pi}{4}\sqrt{\hat{\omega}}\right) \cos\left(\frac{3\pi}{4}\sqrt{\hat{\omega}}\right).$$

The fundamental difference with Secs. III and IV is the presence of terms depending on the frequency. They are written as functions of the dimensionless frequencies $\hat{\omega}_w$ and $\hat{\omega}_f$. The first one $\hat{\omega}_w$ is equal to the ratio between ω, the circular frequency, and ω_{w1}, the circular frequency of the first bending mode of the walls with two fixed ends. Similarly $\hat{\omega}_f$ corresponds to the ratio between ω and ω_{f1}, the circular frequency of the first bending mode of the floors with two fixed ends. Moreover, the natural frequencies of a beam that is fixed at both extremities are the solutions of the following equation:

$$2 f_o(\hat{\omega}) f_e(\hat{\omega}) = 1 - \cos\left(\frac{3\pi}{2}\sqrt{\hat{\omega}}\right) \cosh\left(\frac{3\pi}{2}\sqrt{\hat{\omega}}\right) = 0,$$

where the function f_o vanishes at the frequencies of the odd bending modes and the function f_e vanishes at the frequencies of the even bending modes.

($x0$) and ($y0$) of Eq. (17) contain the same elastic terms as in Sec. III, which are related to the tension-compression of the elements. In addition, there are the inertial terms the order of magnitude of which has changed due to the increase of the frequency. Because of the local resonance in bending, the real mass is replaced by an *effective mass depending on the frequency and the direction*. ($x0$) of Eq. (17) describes the momentum balance when the floors experience tension-compression and the walls experience resonance as presented in Fig. 5. Therefore the mass of the walls M_w is multiplied by a frequency dependent function f giving an effective mass. In ($y0$) of Eq. (17), the roles of the walls and the floors are reversed, and the function f modifies the mass of the floors M_f. As for ($m0$) of Eq. (17), at lower frequencies, it gives the equality of the macroscopic shear stresses associated to the bending of the elements. Consequently this equation is strongly affected by the local resonance. Nevertheless it still expresses the inner equilibrium of the basic frame and it enables to calculate the "hidden" variable $\tilde{\theta}^0$.

In the sequel, the study focuses on ($x0$) and ($y0$) of Eq. (17), which describe the wave propagation. First, the type of waves and the influence of the direction of propagation $\boldsymbol{n}_\alpha$ are determined. Then the properties of the effective mass are examined. Finally, ($m0$) of Eq. (17) which imposes additional kinematic conditions, is considered.

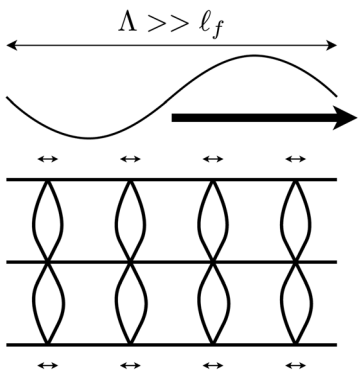

FIG. 5. Compressional wave in the floors ⇒ resonance in bending of the walls.

A. Effect of the anisotropy

The analysis of the wave propagation is carried out using the same method as in Sec. IV. Expression (13) of the displacement field is introduced in ($x0$) and ($y0$) of Eq. (17):

$$\left(-E_x k^2(\alpha)\cos^2(\alpha) + M^w(\hat{\omega}_w)\omega^2\right) \tilde{u}_x^0 \exp[-ik(\alpha)\boldsymbol{n}_\alpha \cdot \boldsymbol{x}] = 0 \qquad (x0)$$

$$\left(-E_y k^2(\alpha)\sin^2(\alpha) + M^f(\hat{\omega}_f)\omega^2\right) \tilde{u}_y^0 \exp[-ik(\alpha)\boldsymbol{n}_\alpha \cdot \boldsymbol{x}] = 0 \qquad (y0) \qquad (18)$$

$$\text{with} \quad M^w(\hat{\omega}_w) = M_f + M_w f(\hat{\omega}_w)$$
$$M^f(\hat{\omega}_f) = M_w + M_f f(\hat{\omega}_f).$$

The existence of a non-zero solution implies that:

$$-E_x k^2(\alpha)\cos^2(\alpha) + M^w(\hat{\omega}_w)\omega^2 = 0 \qquad (19a)$$

$$\text{or} \quad -E_y k^2(\alpha)\sin^2(\alpha) + M^f(\hat{\omega}_f)\omega^2 = 0. \qquad (19b)$$

When Eq. (19a) is satisfied, then $\tilde{u}_y^0 = 0$, and all the nodes move in the x direction [Fig. 6(a)]. Conversely, when Eq. (19b) is satisfied, then $\tilde{u}_x^0 = 0$, and all the nodes move in the y direction [Fig. 6(b)]. These two modes of polarization are called X-mode and Y-mode, respectively.

Equation (19a) shows that the X-mode can exist for waves traveling in all directions except in the y direction [$\cos(\alpha) = 0$]. For waves traveling in the x direction ($\alpha = 0$), the direction of propagation and the direction of polarization are identical. They are pure compressional waves with the following properties:

$$k(0) = \omega\sqrt{\frac{M^w(\hat{\omega}_w)}{E_x}} \quad \Rightarrow \quad c(0) = \sqrt{\frac{E_x}{M^w(\hat{\omega}_w)}}. \qquad (20)$$

The speed $c(0)$ is similar to the one of a compressional wave in a classical elastic medium provided that the real mass is replaced by the effective mass.

The X-mode waves traveling diagonally are shear-compression waves. This type of waves is frequently encountered in anisotropic media. Here the particularity is that the direction of polarization is independent of the direction of propagation. It is just imposed by the orientation of the elements. However, the properties of the X-mode waves strongly vary with the direction of propagation:

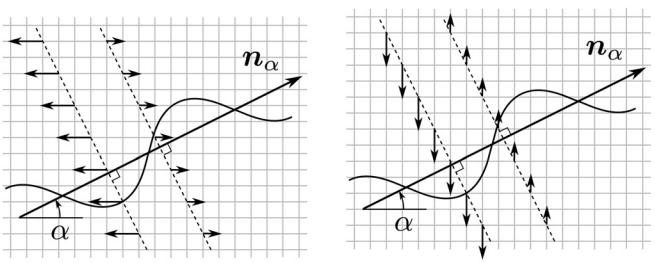

FIG. 6. Nodal displacements for the two modes of polarization.

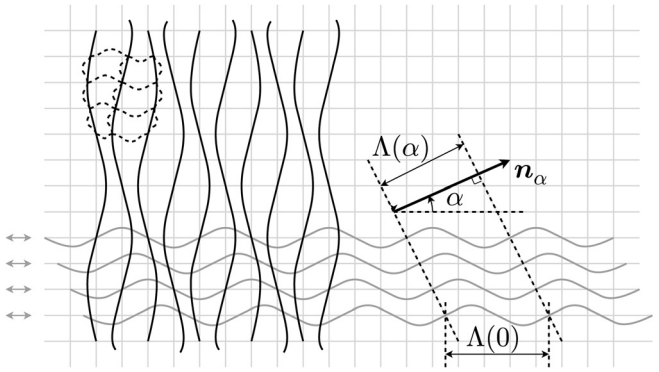

FIG. 7. Description of the mechanisms which generate a macroscopic shear-compression wave traveling in the direction $\boldsymbol{n}_\alpha$ with the X-mode.

$$k(\alpha) = \frac{k(0)}{|\cos(\alpha)|} \quad \Rightarrow \quad c(\alpha) = |\cos(\alpha)|c(0).$$

The mechanisms at the microscopic scale governing these waves are explained in Fig. 7. The gray grid represents the structure before deformation. All the nodal displacements are in the x direction, as shown by the arrows on the left. The motions are caused by the propagation of pure compressional waves in the floors that are out-of-phase, so that all the points on a straight line perpendicular to the direction $\boldsymbol{n}_\alpha$ have the same displacement. As a result, at the macroscopic scale, a wave traveling in the direction $\boldsymbol{n}_\alpha$ is observed. The amplitude of the compressional waves in the floors is represented by the gray sinusoids at the bottom of the figure. Their wavelength is $\Lambda(0) = 2\pi/k(0)$. The wavelength of the macroscopic wave $\Lambda(\alpha)$ is the projection of $\Lambda(0)$ onto the direction $\boldsymbol{n}_\alpha$. Consequently the wavelength (and therefore the speed) is maximal when the macroscopic wave travels in the x direction. Moreover, this mechanism cannot generate a macroscopic wave traveling in the y direction. The vertical black sinusoids represent the deformation of the walls due to the phase difference between the compressional waves in the floors. The total deformation is obtained by adding the deflections induced by the local resonance (drawn with dotted lines on the top left corner).

For the Y-mode, the roles of the floors and the walls are reversed. Macroscopic waves with the following properties can travel in all directions except in the x direction:

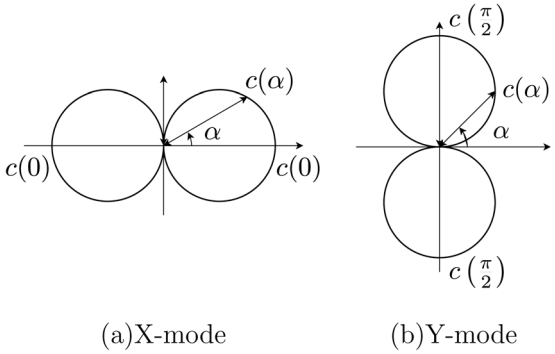

FIG. 8. Variations of the speed of the macroscopic waves according to the direction of propagation.

$$k\left(\frac{\pi}{2}\right)=\omega\sqrt{\frac{M^f(\hat{\omega}_f)}{E_y}} \quad \Rightarrow \quad c\left(\frac{\pi}{2}\right)=\sqrt{\frac{E_y}{M^f(\hat{\omega}_f)}}$$

$$k(\alpha)=\frac{k\left(\frac{\pi}{2}\right)}{|\sin(\alpha)|} \quad \Rightarrow \quad c(\alpha)=\left|\sin(\alpha)\right|c\left(\frac{\pi}{2}\right). \qquad (21)$$

Figure 8 sums up the variations of the speed of the macroscopic waves for the two modes of polarization.

B. Effect of the local resonance

The influence of frequency is now investigated. To simplify, walls and floors are assumed perfectly identical. Thus subscripts "*w*" and "*f*" can be removed. The dimensionless mass $m(\hat{\omega})$ is defined by the ratio between the effective mass and the real mass:

$$m(\hat{\omega})=\frac{M(\hat{\omega})}{M_s}=\frac{\frac{\bar{\rho}}{\ell}(1+f(\hat{\omega}))}{2\bar{\rho}/\ell}=\frac{1}{2}(1+f(\hat{\omega})),$$

where $\hat{\omega}\approx\omega/\omega_1$ is the ratio between ω and the circular frequency of the first bending mode of the elements with two fixed ends. The dimensionless mass is plotted in Fig. 9. As the frequencies of the bending modes of Euler–Bernoulli beams are proportional to the sequence of the squares of the odd integers, the modes of the elements correspond to the following abscissas:

$$\hat{\omega}_1\approx\frac{3^2}{3^2}=1, \quad \hat{\omega}_2\approx\frac{5^2}{3^2}\approx 2.78, \quad \hat{\omega}_3\approx\frac{7^2}{3^2}\approx 5.44,\ldots.$$

Figure 9 shows that the limit of the effective mass at very low frequencies is the real mass as expected. At most of the frequencies higher than the one of the first bending mode of the elements, $m(\hat{\omega})$ is between 0 and 1. This means that the structure seems lighter thanks to the local resonance. On the contrary, close to the frequencies of the odd bending modes of the elements, the effective mass becomes infinite and changes its sign. Such an atypical behavior is not observed close to the frequencies of the even bending modes.

The effective mass differs significantly from the real mass because the points of the cell are in relative motion. According to the definition of the macroscopic variables, the

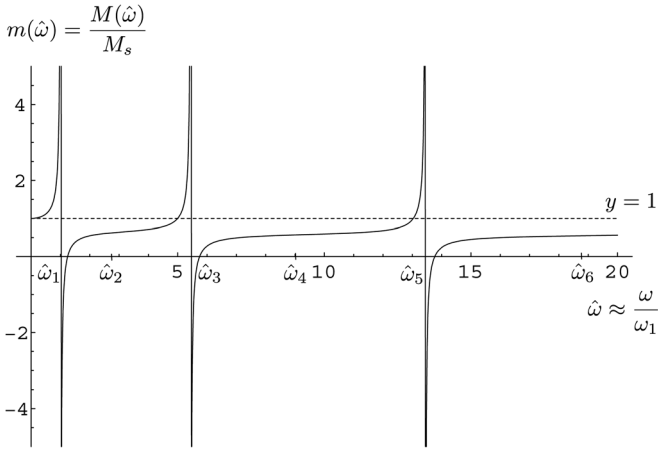

FIG. 9. Variations of the effective mass according to the frequency.

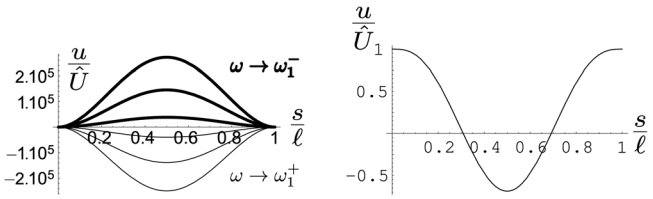

(a) $\omega\to\omega_1$ (b) $\omega=\omega_2$

FIG. 10. Deflection u of a wall caused by the propagation of a wave in the x direction with the X-mode. $\hat{U}$ is the amplitude of the motion of the nodes, s is the coordinate along the axis of the wall, and ℓ is the length of the wall.

macroscopic wave describes the motion of the nodes. At low frequencies, the whole cell undergoes the same translational motion. Consequently, the sum of inertia forces acting on the whole frame equals the real mass of the frame multiplied by the acceleration of the nodes. When bending resonance occurs, the motion of the other points can strongly differ from the one of the nodes and some points can even be in antiphase. In these conditions, the sum of inertia forces acting on the basic frame is more complex.

This analysis of the physical origin of the effective mass is verified by calculating the deformation of a wall caused by the propagation of a macroscopic wave in the x direction with the X-mode. In that case, the extremities of the wall move in-phase in the transverse direction. Moreover, ($m0$) of Eq. (17) shows that there is no rotation of the nodes. The ratio between u the amplitude of the deflection of the wall and $\hat{U}$ the amplitude of the motion of the nodes is plotted in Fig. 10. As ω approaches ω_1, the circular frequency of the first bending mode of the wall [Fig. 10(a)], the deflection is getting larger and larger because of the resonance. It is in-phase with the nodes when ω is below ω_1 and in antiphase when ω is above ω_1. At the frequency of the second bending mode [Fig. 10(b)], the boundary conditions do not cause the resonance of the wall. Nevertheless the motion is not uniform, which induces an effective mass smaller than the real mass. This behavior is consistent with the variations of the effective mass (Fig. 9).

The consequences on the wave propagation are examined by considering a more realistic case with damping. Now the elastic modulus of the material is a complex number: $\hat{E}=|E|e^{i\eta}$ with $0<\eta\ll 1$. In what follows, all calculations will be made with $\eta=2.10^{-2}$. As a result, the effective mass becomes a complex number with a finite modulus. The modulus and the argument are plotted in Fig. 11.

Owing to the variations of the effective mass, there is dispersion of the wave speed. In Fig. 12, the thick line represents $\hat{c}$ the ratio between the speed calculated by taking into account the local resonance and the speed obtained by neglecting this phenomenon. The thin line corresponds to the attenuation per wavelength δ_Λ. This means that the amplitude of the wave is multiplied by $e^{-\delta_\Lambda}$ when it travels one wavelength.

As expected, the limit of $\hat{c}$ at very low frequencies is 1, and $\hat{c}$ decreases when ω approaches ω_1. At most of the circular frequencies higher than ω_1, waves propagate faster thanks to the local resonance. As the frequency approaches the one of an odd bending mode from below, the speed first decreases and then increases considerably. At the same time,

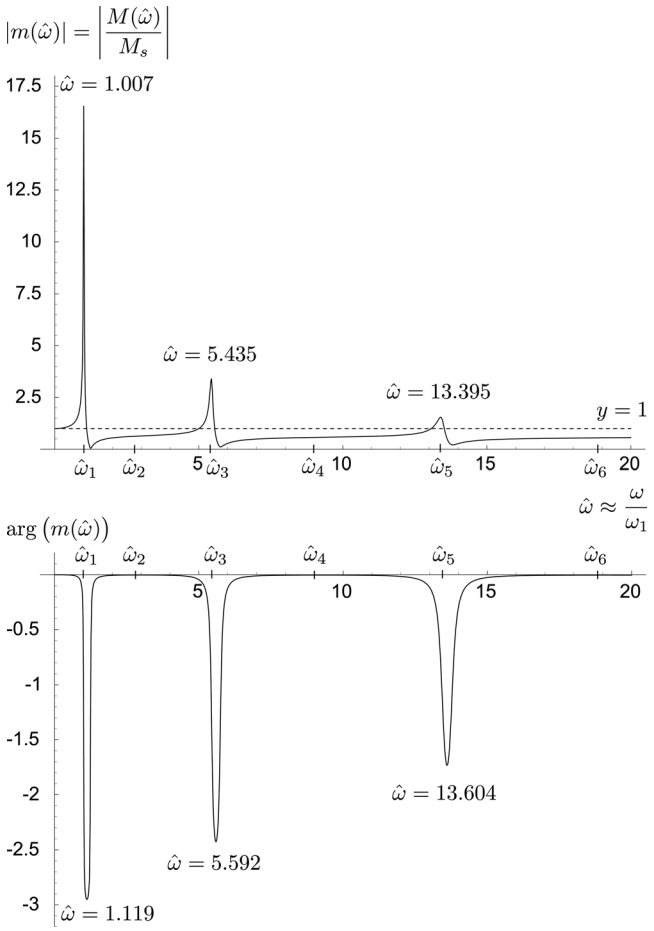

FIG. 11. Modulus and argument of the effective mass in presence of damping ($\eta = 2.10^{-2}$).

δ_Λ becomes very important. Therefore the neighborhood of the odd bending modes of the elements corresponds to *frequency bandgaps*. However, after the resonance frequencies, δ_Λ decreases faster than $\hat{c}$. When δ_Λ becomes negligible, $\hat{c}$ is still significantly higher than 1.

C. Inner equilibrium of the frame

The inner equilibrium of the basic frame is described by $(m0)$ of Eq. (17). The reasoning is illustrated by considering the X-mode, but the same phenomena occur with the Y-mode. Then $(m0)$ of Eq. (17) becomes:

$$\frac{\pi G_w\sqrt{\hat{\omega}_w}}{8 f_e(\hat{\omega}_w)}\left(4\sin\left(\frac{3\pi}{4}\sqrt{\hat{\omega}_w}\right)\sinh\left(\frac{3\pi}{4}\sqrt{\hat{\omega}_w}\right)\tilde{\theta}^0 + \frac{3\pi\sqrt{\hat{\omega}_w}}{2 f_o(\hat{\omega}_w)}\left(\cosh\left(\frac{3\pi}{2}\sqrt{\hat{\omega}_w}\right)-\cos\left(\frac{3\pi}{2}\sqrt{\hat{\omega}_w}\right)\right)\frac{\partial \tilde{U}_x^0}{\partial y}\right) + \frac{\pi G_f\sqrt{\hat{\omega}_f}}{2 f_e(\hat{\omega}_f)}\sin\left(\frac{3\pi}{4}\sqrt{\hat{\omega}_f}\right)\sinh\left(\frac{3\pi}{4}\sqrt{\hat{\omega}_f}\right)\tilde{\theta}^0 = 0.$$

At most of the frequencies, the node rotation $\tilde{\theta}^0$ is proportional to the shear strain $\partial_y \tilde{U}_x^0$ with a rather complicated proportionality coefficient. However, at some frequencies, the functions have singularities and their physical origin is now examined.

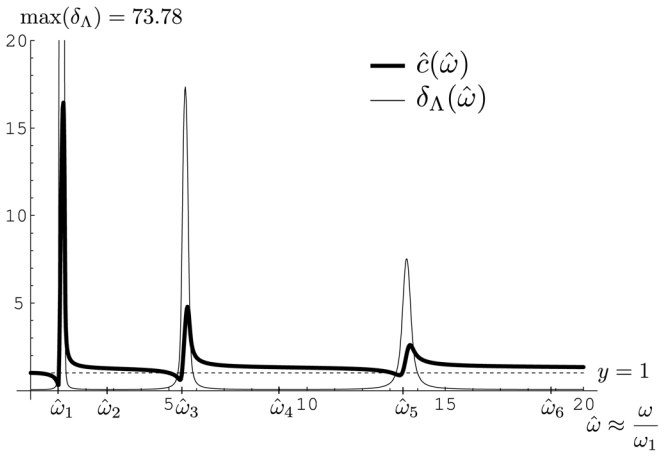

FIG. 12. Speed (thick line) and attenuation per wavelength (thin line) for $\eta = 2.10^{-2}$.

The simplest case corresponds to the very low frequencies. As ω approaches 0, the limit of $(m0)$ of Eq. (17) is identical to the equation of Sec. III that expresses the equality of the macroscopic shear stresses in statics. The frequencies of the odd bending modes of the walls $[f_o(\hat{\omega}_w) = 0]$ can also be eliminated because the wave propagation is impossible for the X-mode due to the local resonance.

Frequencies of the even bending modes of the elements $[f_e(\hat{\omega}_w) = 0$ or $f_e(\hat{\omega}_f) = 0]$ are more interesting. In their neighborhood, the effective stiffness of the elements becomes infinite. This behavior is due to the fact that the boundary conditions of a beam at its natural frequencies are not independent.

Another singularity occurs when the coefficient of $\tilde{\theta}^0$ vanishes. This means that the effective stiffness of the whole cell disappears. Whatever the node rotation $\tilde{\theta}^0$, it generates a negligible moment that cannot balance the moment caused by the shear strain. As a result, there is no shear strain, and the compressional waves in the floors are in-phase.

Even if the wave propagation is described by $(x0)$ and $(y0)$ of Eq. (17), this example shows that it is necessary to verify that the kinematic conditions imposed by $(m0)$ of Eq. (17) are satisfied. Here there are frequencies at which waves cannot propagate diagonally.

VI. BEHAVIOR OF REAL MEDIA

This section explains how the previous results can help to understand the dynamics of real frame structures. It begins with some comments about the scale ratio and the parameter ϵ, which play a key role during the homogenization process. Then a method is proposed for the design of real frame structures with unusual properties.

A. The scale ratio

A macroscopic plane wave with a circular frequency ω traveling in a given frame structure is considered. From a physical point of view, the scale ratio is defined by the ratio between the characteristic length ℓ_c of the basic frame and the characteristic length L of the deformation of the structure. In what follows, the scale ratio ℓ_c/L will be written $\tilde{\epsilon}$ as

in Ref. 28 to make it different from the small parameter ϵ used in homogenization. As ℓ_c and L are finite, the scale ratio is a finite quantity. If $\tilde{\epsilon}$ is small ($\tilde{\epsilon} \ll 1$), it is possible to homogenize the behavior of the structure.

For this purpose, first the powers of $\tilde{\epsilon}$ are used as a kind of "unit of measurement" to convert the numerical values of the other small parameters (in particular the thickness to length ratios of the elements) into orders of magnitude. This provides the proper normalization for the real structure. Second, homogenization consists in replacing in the scaled formulation the physical $\tilde{\epsilon}$ by a mathematical ϵ, which is made to approach zero. In doing so, the relative orders of magnitude of the physical terms are kept identical from the real frame structure to the continuum obtained at the limit.

However, as the physical $\tilde{\epsilon}$ is a finite quantity, the real structure is an imperfect realization of the homogenized model (or the homogenized model is an approximation of the behavior of the real structure). The smaller $\tilde{\epsilon}$ is, the smaller the difference between the model and the structure is. By considering only the leading order as in the previous sections, the order of magnitude of the neglected correctors is $O(\tilde{\epsilon})$.

All this shows that it is important to have a reliable estimation of $\tilde{\epsilon}$ for two reasons: to correctly take into account the physics of the problem and to evaluate the accuracy of the continuous model. For a given structure, the size of the frame ℓ_c is fixed (here $\ell_c = \ell_w$), but the macroscopic length depends on the external actions. In the case of wave propagation, it can be shown[29] that:

$$L = \frac{\Lambda}{2\pi} \quad \Rightarrow \quad \tilde{\epsilon} = \frac{2\pi\ell_c}{\Lambda} = \ell_c k, \tag{22}$$

where Λ is the macroscopic wavelength and k the wave number given by Eq. (16) for pure shear waves, by Eq. (20) for shear-compression waves polarized in the x direction, or by Eq. (21) for shear-compression waves polarized in the y direction. As a result, $\tilde{\epsilon}$ depends on the frequency. When ω increases, Λ decreases. Thus $\tilde{\epsilon}$ becomes greater, and the continuous model is less accurate. Moreover, as the thickness to length ratios of the elements have fixed values, the orders of magnitude given by the normalization change.

The expression of the macroscopic wavelength varies also with the nature of the wave. For example, a shear wave and a compressional wave both traveling in the x direction are considered. The associated wave numbers are given by Eqs. (16) and (20), which are very different. But the thickness to length ratios of the elements are described by Eq. (8) in both cases. If, in addition, these cases apply to the same real structure, the thickness to length ratios have a fixed value. Therefore $\tilde{\epsilon}$, and so Λ and k, should have the same value for the two types of wave. This is possible only when the frequency of the shear wave is smaller than the frequency of the compressional wave. This is the reason why homogenization gives the impression that different types of wave appear in very different frequency ranges, whereas they can coexist in the same frequency range in real structures.

Instead of considering a constant wavelength, another possibility consists in assuming that the frequency is constant. In that case, the wavelength of the shear wave is smaller than the wavelength of the compressional wave, and $\tilde{\epsilon}$ has two different values. As a result, the normalization provides different orders of magnitude, and the real structure is associated with two different continua. Note that the accuracy of the descriptions of the macroscopic waves is also different.

B. Design of metamaterials

The analytical formulation of the HPDM method provides a clear understanding of the mechanisms governing the behavior of frame structures and of the role of each parameter. This constitutes a framework for the design of new (meta)materials with prescribed macroscopic properties.

The reasoning is illustrated by considering the design of a structure that behaves as a metamaterial for pure compressional waves propagating at a given circular frequency ω. To simplify, the basic frame is a perfect square and the walls, and the floors are made of the same given material. Thus subscripts "w" and "f" are removed. The length ℓ of the elements is fixed. The objective is the determination of their thickness a. The normalization (8) and the expression (20) of the wavenumber impose the following condition for the thickness:

$$\frac{a}{\ell} = O(\tilde{\epsilon}) = O(\ell k) = O\left(\ell\omega\sqrt{\frac{M_f + M_w f(\hat{\omega}_w)}{E_x}}\right).$$

The expressions of M_f, M_w, E_x are given in Sec. II E, and the function f is defined in Sec. V. Neglecting the effects of the local resonance [by taking $f(\hat{\omega}_w) = 1$] yields:

$$a = O\left(\ell^2\omega\sqrt{\frac{2\rho A/\ell}{EA/\ell}}\right) = O\left(\ell^2\omega\sqrt{\frac{2\rho}{E}}\right).$$

Thus $a = \hat{a}\ell^2\omega\sqrt{\rho/E}$ where $\hat{a} = O(1)$ is a constant. It is possible to verify that, in that case, the local resonance actually appears close to the circular frequency ω. For $\hat{a} = 1$, the ratio between the bending wavelength in the elements λ_b and their length ℓ is:

$$\frac{\lambda_b}{\ell} = \frac{2\pi}{\ell}\sqrt[4]{\frac{EI}{\rho A\omega^2}} = \frac{2\pi}{\ell}\sqrt[4]{\frac{\mathrm{EAa}^2}{12\rho\mathrm{A}\omega^2}} = 2\pi\sqrt[4]{\frac{1}{12}} \approx 3.38.$$

This corresponds to the beginning of the resonance: ω is a little smaller than the circular frequency of the first bending mode. For the effects of the local resonance to be more marked at ω, a smaller $\hat{a}$ should be chosen. This procedure completely defines the resonating media.

The previous example focuses only on the thickness, but it is also possible to adjust the other geometrical parameters or the material properties to obtain the desired macroscopic properties. For instance, if the waves propagating in the medium are always polarized in the same direction, some mass can be added to the resonating elements to increase the effects of the local resonance. However, when the walls and the floors are different, the stiffness contrast should remain small. Otherwise, a new mechanism appears in the structure and the macroscopic description is no longer valid.[28,30]

Although the results are obtained for a specific class of structures, their generalization is straightforward for three-dimensional frame structures and structures the unit cell of which is a parallelogram. For braced structures such as triangular lattices, the high contrast between the shear and tension-compression deformabilities is lost. The mechanism identified for the shear waves probably no longer exists. However, compressional waves can presumably be associated with local resonance in bending. Note that macroscopic beam models obtained with the HPDM method have been successfully applied to real buildings.[31]

VII. CONCLUSION

Thanks to the contrast between the bending and tension-compression properties of the Euler–Bernoulli beams, the homogenization method of periodic discrete media (HPDM) is extended to higher frequencies with local resonance in bending. This method is used for the study of the wave propagation in two-dimensional frame structures. Its main advantage is the analytical formulation that enables to understand the mechanisms governing the global behavior.

When all the elements of the basic frame have similar properties and in the absence of local resonance, the equivalent continuum at the macroscopic scale is a "classical" continuum in the sense that the only kinematic variables are the translational motions of the nodes and therefore of the whole cell. However, the continuum is highly anisotropic. It has different elastic moduli according to the frame axes and a shear modulus much lower than the elastic moduli. In consequence, the speed of the waves strongly depends on the direction. Moreover, shear waves appear at lower frequencies than shear-compression waves and two frequency ranges should be studied.

For shear waves, elements have a quasi-static behavior at the local scale for both mechanisms: bending and tension-compression. It corresponds to the usual domain of application of homogenization. Shear waves are generated by the local bending of the elements. They can travel only in the two discrete directions of the frame elements with the same speed. The speed is also independent of the frequency.

For shear-compression waves, elements have a quasi-static behavior at the local scale for tension-compression and a dynamic behavior for bending. Therefore the behavior of the structure should be homogenized with the new procedure adapted to local resonance. Shear-compression waves can travel in all the directions, but their direction of polarization coincides with those of the elements. Indeed the macroscopic waves are generated at the local scale by the propagation of compressional waves in the elements. The main consequence of the local resonance is that the real mass of the cell has to be replaced by an effective mass that depends on the frequency and the direction of polarization. As a result, the speed of the macroscopic waves also varies with the frequency and the direction of polarization. Moreover the speed depends on the direction of propagation.

The effective mass exhibits different properties depending on whether the frequency is smaller or greater than ω_1, the frequency of the first bending mode of the elements affected by the resonance. At very low frequencies, the effective mass is equal to the real mass. When the frequency is increased but remains smaller than ω_1, the effective mass increases too, which leads to a decrease of the speed of the macroscopic waves. This behavior is consistent with the experimental results concerning the Rayleigh scattering. At frequencies close to ω_1 (and the frequencies of the other odd bending modes), the inertia forces become huge because of the resonance. Therefore the effective mass approaches infinity, which causes frequency bandgaps.

After the resonance, at most of the frequencies higher than ω_1, the effective mass is smaller than the real mass and waves travel faster due to the dynamic effects at the local scale. This domain is intermediate between the domain of the Rayleigh scattering (when the wavelength is much greater than the cell size and the local dynamic effects are negligible) and the domain of the various phenomena observed in phononic crystals such as Bragg scattering, focusing of waves[32].... In this latter case, the wavelength is comparable to the cell size.

At the frequencies of the even bending modes, the effective mass has a finite value because these modes are not excited by the propagation of the macroscopic waves. However, the effective stiffness of the elements becomes infinite. This is due to the kinematic incompatibility between the macroscopic waves and the boundary conditions of the elements.

As other periodic media, frame structures behave as frequency and spatial filters. In the present case, the spatial properties are particularly pronounced because the waves are channeled by the elements. Concerning the frequency properties, the features of the effective mass are similar to those of the effective masses obtained for other metamaterials consisting either of composite media with a high contrast between the rigidities of the constituents[6] or of hard spheres coated with a soft material and dispersed in a stiff matrix.[10,33] Here another approach to create such materials is proposed. It is based on the stiffness contrast between bending and tension-compression in beams instead of the contrast between the mechanical properties of different materials. Moreover, the HPDM method being completely analytic, the results can be easily used to design new metamaterials.

As mentioned in the introduction, the concept of local resonance in highly contrasted elastic composites has been evidenced by Auriault and Bonnet in 1985 (Ref. 6) by means of the homogenization of periodic media with an heuristic approach and formal expansions. Similar mechanisms were also identified in double conductivity media[34] and double porosity media (e.g., Refs. 35 and 36) and were proved experimentally in acoustics.[37] In these latter cases, the difference lies in the fact that the resonance concerns a diffusion phenomenon (related to thermal transfer or mass transfer driven by viscous effects). In the same spirit, one may also consider that the local mechanism expressed by the dynamic permeability of porous media,[38,39] relevant when the thickness of the viscous layer interferes with the pore size, belongs to the same family of phenomena. Undamped resonance (as in elastic cases) or damped resonance (as in diffusion cases) obviously results in different macroscopic modeling. However, the common feature of these several

situations is that they lead at the macroscopic scale to a generalized Newtonian mechanics in the sense that the effective mass (or thermal inertia, etc.) differs from the actual mass of the real system.

Interestingly, the theoretical mathematical study of the local elastic resonance mechanism has been investigated significantly later than the heuristic results on realistic materials. The work of Zhikov[40] provides results on the convergence of the asymptotic approach. Note also that the present work focuses on local resonance when the scale separation is satisfied. For this reason, it differs from the theories currently developed in Refs. 24–26 to derive a macroscopic modeling at high frequencies, i.e., when the scale separation in the usual sense is no longer satisfied.

Finally, there probably exists other types of waves different from the two types described here. For this first study, the kinematic variables periodicity is identical to the geometric periodicity. However, other researches on the extension of homogenization to higher frequencies[24–26,41] suggest that this hypothesis is too restrictive and that the kinematic variables are often periodic on two cells. Another possible continuation of the present work could be the study of structures with walls different from the floors or with a different cell geometry.

[1]L. Brillouin, *Wave Propagation in Periodic Structures* (McGraw-Hill, New York, 1946).
[2]D. J. Mead, "Wave propagation in continuous periodic structures: Research contributions from Southampton, 1964–1995," J. Sound Vib. **190**, 495–524 (1996).
[3]R. S. Langley, N. S. Bardell, and H. M. Ruivo, "The response of two-dimensional periodic structures to harmonic point loading: A theoretical and experimental study of a beam grillage," J. Sound Vib. **207**, 521–535 (1997).
[4]M. Ruzzene, F. Scarpa, and F. Soranna, "Wave beaming effects in two-dimensional cellular structures," Smart Mater. Struct. **56**, 363–372 (2003).
[5]A. Srikantha Phani, J. Woodhouse, and N. A. Fleck, "Wave propagation in two-dimensional periodic lattices," J. Acoust. Soc. Am. **119**, 1995–2005 (2006).
[6]J.-L. Auriault and G. Bonnet, "Dynamique des composites élastiques périodiques (Dynamics of periodic elastic composites)," Arch. Mech. **37**, 269–284 (1985).
[7]P. G. Martinsson and A. B. Movchan, "Vibrations of lattice structures and phononic band gaps," Q. J. Mech. Appl. Math. **12**, 45–64 (2003).
[8]Z. Liu, X. X. Zhang, Y. W. Mao, Y. Y. Zhu, Z. Y. Yang, C. T. Chan, and P. Sheng, "Locally resonant sonic materials," Science **289**, 1734–1736 (2000).
[9]Y. Shanshan, Z. Xiaoming, and H. Gengkai, "Experimental study on negative effective mass in a 1D mass-spring system," New J. Phys. **10**, 11 (2008).
[10]Y. Wu, Y. Lai, and Z.-Q. Zhang, "Effective medium theory for elastic metamaterials in two dimensions," Phys. Rev. B **76**, 205313–205320 (2007).
[11]G. W. Milton and J. R. Willis, "On modifications of Newton's second law and linear continuum elastodynamics," Proc. R. Soc. A **463**, 855–880 (2007).
[12]G. A. Maugin and A. V. Metrikine, eds., *Mechanics of Generalized Continua—One Hundred Years After the Cosserats. Advances in Mechanics and Mathematics* (Springer, New York, 2010), Vol. **21**.
[13]Z. P. Bazant and M. Christensen, "Analogy between micropolar continuum and grid frameworks under initial stress," Int. J. Solids Struct. **8**, 327–346 (1972).
[14]A. K. Noor, "Continuum modeling for repetitive lattice structures," Appl. Mech. Rev. **41**, 285–296 (1988).
[15]I. Andrianov, "The specific features of the limiting transition from a discrete elastic medium to a continuous one," J. Appl. Math. Mech. **66**, 261–265 (2002).
[16]A. Bensoussan, J.-L. Lions, and G. Papanicolaou, *Asymptotic Analysis for Periodic Structures. Studies in Mathematics and its Applications* (North Holland, Amsterdam, 1978), Vol. **5**.
[17]E. Sanchez-Palencia, *Non-Homogeneous Media and Vibration Theory. Lecture Notes in Physics* (Springer-Verlag, Berlin, 1980), Vol. **127**.
[18]N. S. Bakhvalov and G. P. Panasenko, *Homogenization: Averaging Processes in Periodic Media* (Nauka, Moscou, 1984) (in Russian), English translation (Kluwer, Dordrecht, 1989).
[19]C. Boutin and J -L. Auriault, "Rayleigh scattering in elastic composite materials," Int. J. Eng. Sci. **31**, 1669–1689 (1993).
[20]D. Cioranescu and J. Saint Jean Paulin, *Homogenization of Reticulated Structures. Applied Mathematical Sciences* (Springer-Verlag, New York, 1999), Vol. **136**.
[21]R. Chiheb, D. Cioranescu, A. El Janati, and G. Panasenko, "Reinforced reticulated structures in elasticity," C. R. Acad. Sci., Ser. I: Math. **326**, 897–902 (1998).
[22]D. Caillerie, P. Trompette, and P. Verna, "Homogenisation of periodic trusses," in *IASS Symposium, 10 Years of Progress in Shell and Spatial Structures* (Madrid, 1989).
[23]H. Tollenaere and D. Caillerie, "Continuous modeling of lattice structures by homogenization," Adv. Eng. Softw. **29**, 699–705 (1998).
[24]N. Moustaghfir, E. M. Daya, B. Braikat, N. Damil, and M. Potier-Ferry, "Evaluation of continuous modelings for the modulated vibration modes of long repetitive structures," Int. J. Solids Struct. **44**, 7061–7072 (2007).
[25]R. V. Craster, J. Kaplunov, and A. V. Pichugin, "High-frequency homogenization for periodic media," Proc. R. Soc. A **466**, 2341–2362 (2010).
[26]R. V. Craster, J. Kaplunov, and J. Postnova, "High-frequency asymptotics, homogenisation and localisation for lattices," Q. J. Mech. Appl. Math. **63**, 497–519 (2010).
[27]C. Boutin and S. Hans, "Homogenisation of periodic discrete medium: Application to dynamics of framed structures," Comput. Geotech. **30**, 303–320 (2003).
[28]S. Hans and C. Boutin, "Dynamics of discrete framed structures: A unified homogenized description," J. Mech. Mater. Struct. **3**, 1709–1739 (2008).
[29]C. Boutin and J.-L. Auriault, "Dynamic behaviour of porous media saturated by a viscoelastic fluid. Application to bituminous concretes," Int. J. Eng. Sci. **28**, 1157–1181 (1990).
[30]C. Chesnais, "Dynamique de milieux réticulés non contreventés—Application aux batiments (Dynamics of unbraced reticulated media—Application to buildings)," Ph.D. thesis, ENTPE - ECL (2010), http://bibli.ec-lyon.fr/exl-doc/TH_T2177_cchesnais.pdf (Last viewed 8/24/2012).
[31]C. Chesnais, C. Boutin, and S. Hans, "Structural dynamics and generalized continua" in *Mechanics of Generalized Continua. Advanced Structured Materials*, edited by H. Altenbach, G. A. Maugin, and V. Erofeev (Springer Berlin, 2011), Vol. **7**, pp. 57–76.
[32]S. Yang, J. H. Page, Z. Liu, M. L. Cowan, C. T. Chan, and P. Sheng, "Focusing of sound in a 3D phononic crystal," Phys. Rev. Lett. **93**, 024301 (2004).
[33]Z. Liu, C. T. Chan, and P. Sheng, "Analytic model of phononic crystals with local resonances," Phys. Rev. B **71**, 014103 (2005).
[34]J.-L. Auriault, "Effective macroscopic description for heat-conduction in periodic composites," Int. J. Heat Mass Transfer **26**, 861–869 (1983).
[35]J.-L. Auriault and C. Boutin, "Deformable porous media with double porosity. Quasi-statics. II: Memory effects," Transp. Porous Media **10**, 153–169 (1993).
[36]C. Boutin, P. Royer, and J.-L. Auriault, "Acoustic absorption of porous surfacing with dual porosity," Int. J. Solids Struct. **35**, 4709–4737 (1998).
[37]X. Olny and C. Boutin, "Acoustic wave propagation in double porosity media," J. Acoust. Soc. Am. **114**, 73–89 (2003).
[38]M. A. Biot, "Theory of propagation of elastic waves in a fluid-saturated porous solid. II. Higher frequency range," J. Acoust. Soc. Am. **28**, 179–191 (1956).
[39]J.-L. Auriault, "Dynamic behavior of a porous medium saturated by a Newtonian fluid," Int. J. Eng. Sci. **18**, 775–785 (1980).
[40]V. V. Zhikov, "On an extension of the method of two-scale convergence and its applications," Mat. Sb. **191**, 973–1014 (2000).
[41]I. L. Manevitch and G. V. Oshmyan, "An asymptotic study of the linear vibrations of a stretched beam with concentrated masses and discrete elastic supports," J. Sound Vib. **223**, 679–691 (1999).
[42]C. Chesnais, S. Hans, and C. Boutin, "Wave propagation and diffraction in discrete structures: Effect of anisotropy and internal resonance," PAMM **7**, 1090401–1090402 (2007), in 6th International Congress on Industrial and Applied Mathematics, Zürich, Switzerland (July 16–20 2007).